Discover Geoscience

RESEARCH Open Access

Inventory of paraglacial slope instabilities following glacier retreat in Venosta Valley, Italy

Michele Di Biase[1*], Chiara Crippa[2], Mattia Callegari[2], Massimiliano Pittore[3] and Davide Fugazza[1]

*Correspondence:
Michele Di Biase
michele.dibiase@unimi.it
[1]Department of Environmental Science and Policy, Università degli Studi di Milano, Milano, Italy
[2]Institute for Earth Observation, Eurac Research, Bolzano, Italy
[3]Center for Climate Change and Transformation, Eurac Research, Bolzano, Italy

Abstract

In the context of climate change, glaciers in the Alps are rapidly receding. Different studies suggest that in this epoch, they are out of balance with the climate, and that glacier retreat rates have exceeded historical precedents from the early 21st century. Mountain glaciers are important resources for society because they provide different ecosystem services. Climate change is threatening the stability of these benefits, and, as a result of permafrost thaw and post-glacial debuttressing, it is causing the emergence of climate-related hazards at high altitude. To understand how mountain slopes react to deglaciation, we compiled the first inventory of paraglacial slope instability phenomena that have occurred on glaciers in the Venosta Valley (Italy) since the Little Ice Age (LIA). We mapped their geographical distribution, evaluated their relationship with deglaciation, and examined their runout to assess the potential implications of such events for alpine routes. To better quantify deglaciation, we also digitized the outlines of the glaciers based on imagery from 2020, updating the archives and providing valuable data for comparison with previous studies. Between 2000 and 2020, a total of 500 slope instability events occurred within a region that, since the LIA, has experienced strong glacier area contraction (-69.44%). This research demonstrates how the mountains are rapidly responding to climate change and deglaciation, highlighting that alpine routes crossing the glaciers in our study region cannot be considered outside the potential runout zone of a rockfall.

Keywords Paraglacial activity, Glacier retreat, Rockfalls, Remote sensing, Climate change

1 Introduction

Glaciers are recognized as indicators of climate change, and their decreasing size and volume are considered an undeniable sign of global warming. Glacier retreat rates have increased since the 1980s and have been exceeding historical precedents in the early 21st century [1, 2]. This trend is observed all over the Alps: the Swiss Glacier Inventory 2010 [3] reports a glacier area loss of 27.7% since 1973 and the extinction of 733 glaciers over the same period; Lambrecht and Kuhn [4] estimated that Austrian glacier area decreased by about 17% during 1969–1998; Knoll and Kerschner [5] reported an area decrease for the South Tyrol glaciers of approximately 36% between 1983 and 2006. In Italy, the last official glacier inventory [6] reported a reduction of approximately 30% in glacier cover

since the 1960s. Considering the whole Alps [7], report a 14% reduction in glacier area between 2003 and 2015. The recession is also evident in the annual reports published at the end of seasonal monitoring of Alpine glaciers. For example, in 2023, glaciers in every Italian region reported losses [8]; a similar situation is observed also in Austria [9] and Switzerland [10]. These data confirm that the regression is common across the Alps and that it is now possible to observe significant glacier variations within an average human lifetime. For this reason, glaciers are often considered valuable indicators of climate variability. In addition, glaciers provide a range of ecosystem services: they are not only strategic water resources for agriculture and hydroelectricity, but also important attractions for alpinists and tourists. Climate change is threatening the stability of these benefits and causing numerous climate-related hazards at high altitudes. On the one hand, the rapid melting and increased availability of liquid water on the glacier surface and at its base are impacting the structural stability of glacier sectors, as seen in the Marmolada collapse [11]. On the other hand, direct effects are also evident in the surrounding rock walls and slopes that, once ice-bonded, are now becoming more unstable due to the reduced geotechnical and mechanical properties of the rock, debris, and soils [12, 13].

These glacial and paraglacial instabilities pose not only a threat to the safety of high-altitude areas but also cause debris to be released over glaciers, modifying their surface properties (e.g., albedo), which, in turn, influences their energy balance and melting rates in a feedback loop (Fig. 1) [14–16].

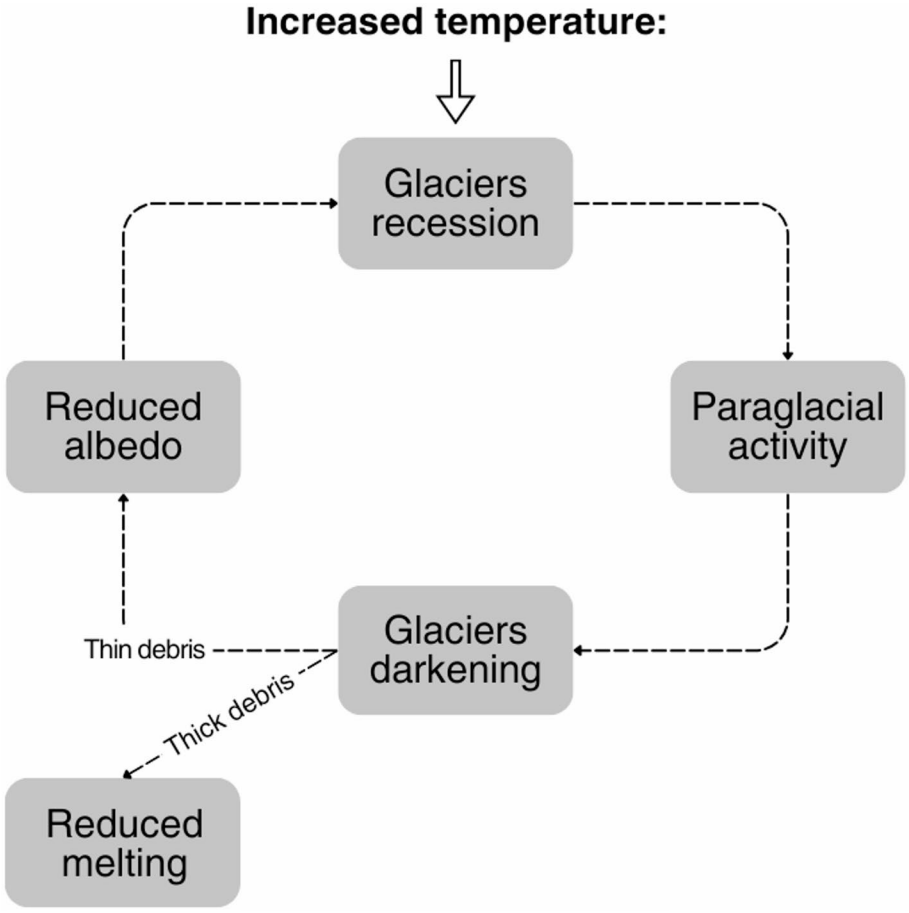

Fig. 1 Scheme of the feedback loop between glacier recession, paraglacial activity, and glacier albedo

At high altitudes, in addition to glacial retreat in the strict sense, permafrost degradation is another major driver of erosion processes. As reviewed in different studies [17–19], changes in ground-ice permafrost temperature act as triggering factors for rockfalls. This destabilization may occur due to three main processes: (I) the fracturing of rock during seasonal and multiannual freezing, (II) changes in hydraulic conductivity, pore water pressure, and circulation during freezing and thawing, and (III) changes in surface geometry resulting from major rockfalls.

The combination of rapid deglaciation with factors such as temperature changes, geological and hydrological settings, enhances the occurrence of slope instability and, therefore, increases the vulnerability of infrastructure and society in general.

While there is a good understanding of the geomechanical processes that trigger glacier-related instabilities, knowledge of their spatio-temporal distribution and their relationship with deglaciation remains limited [16, 20, 21]. In the European Alps, studies have focused on specific events and glaciers, such as those in the Mount Blanc massif [22] and the Great Aletsch Glacier [23]. [24] investigated the Central-Western Alps, but identified only 56 major events because they considered only those with an estimated volume of more than 1000 m^3; smaller events occur even more often but are less easy to recognize.

The limited number of inventories covering entire regions or valleys complicates the study of correlations between paraglacial activity and deglaciation, and the assessment of areas more susceptible to instability. Indeed, as reported by [25], inventories can serve as proxies for analyzing potential predisposing factors or vulnerable infrastructure. In addition, there is an increasing concern among alpinists because instability is altering the accessibility of normal routes, making them increasingly dangerous (e.g., Couloir du Goûter on Mt. Blanc [26, 27]). For alpinists, it is thus relevant to know the frequency and location of slope instabilities, as well as the potential intersection between their runout and the alpine trail. Together with the identification of the release areas, the runout, defined as the process area of the coherent mass discharged during an instability event, is also a key parameter to be estimated, allowing to understand not only the spatial distribution but also the dimensions of the events [28, 29].

Considering all these reasons, compiling inventories is important not only from a scientific perspective but also to describe the state of paraglacial activity in the Alps and aid in the analysis of accessibility in high-altitude areas.

This study aimed to compile an inventory of slope instability events originating from paraglacial mountain sides in the Ortles-Cevedale and Italian Ötztal Group that displaced material onto glacier surfaces up to 2020. At this stage, only phenomena identifiable through aerial and satellite imagery were mapped, as no field surveys or ground-based investigations were conducted. Through this research, we reconstructed the evolution of the glaciers, updated their outlines to 2020, and identified those particularly susceptible to rockfalls. In addition, we focused on rockfall events to analyse their runout using various approaches and to investigate potential interactions with alpine routes or strategic infrastructure (e.g., mountain huts, ski slopes, ski lifts). The compilation of such an inventory is thus important not only from a scientific standpoint, as it assesses the state of paraglacial activity in the Alps, but also for supporting the analysis of accessibility to high-altitude areas and as a fundamental starting point for further detailed analyses.

This research aims to compensate for this gap by providing the first inventory of paraglacial activity in the Venosta Valley (Italy). We strive to describe phenomena that help explain the spatial distribution of rockfalls and the impact of recent high-altitude deglaciation on their occurrence. A detailed inventory of rockfalls in a paraglacial environment has been proposed by [25] for the Ötztal group on the Austrian side; given its framework, we decided to use it as a reference to conduct some comparisons with our study.

1.1 Study area

This research was conducted in the Autonomous Province of South Tyrol (Alto Adige), Italy. More precisely, we focused on the glaciers located in the Ortles-Cevedale massif and the Italian Ötztal Group (Fig. 2a-c). South Tyrol is a mountainous province, and according to the latest official Italian glacier inventory, it is the third-largest Italian region in terms of glacier extension, covering 84.58 km² [6].

The Adige River flows through the Venosta Valley, collecting water from tributary valleys where our glaciers are located. Within our area of interest, the highest peaks are: Ortler/Ortles (3905 m a.s.l.), Königspitze/Gran Zebrù (3851 m a.s.l.), Zufallspitze/Cevedale (3769 m a.s.l.), and Weißkugel/Palla Bianca (3738 m a.s.l.).

Regarding climate, between 1966 and 2015, South Tyrol experienced a significant increase in summer temperatures (+ 2.2 °C) [30]. The topography significantly influences precipitation distribution in the province; specifically, the Venosta Valley is among the driest areas of South Tyrol, with an annual rainfall of approximately 530 mm [31].

The geology of Bolzano province is varied and complex (see Fig. 3) due to the different geological settings that characterized the Alpine orogeny in this sector. From a general perspective, the central-eastern part is mainly characterized by sedimentary and metasedimentary rocks of the South Alpine domain. The western regions are

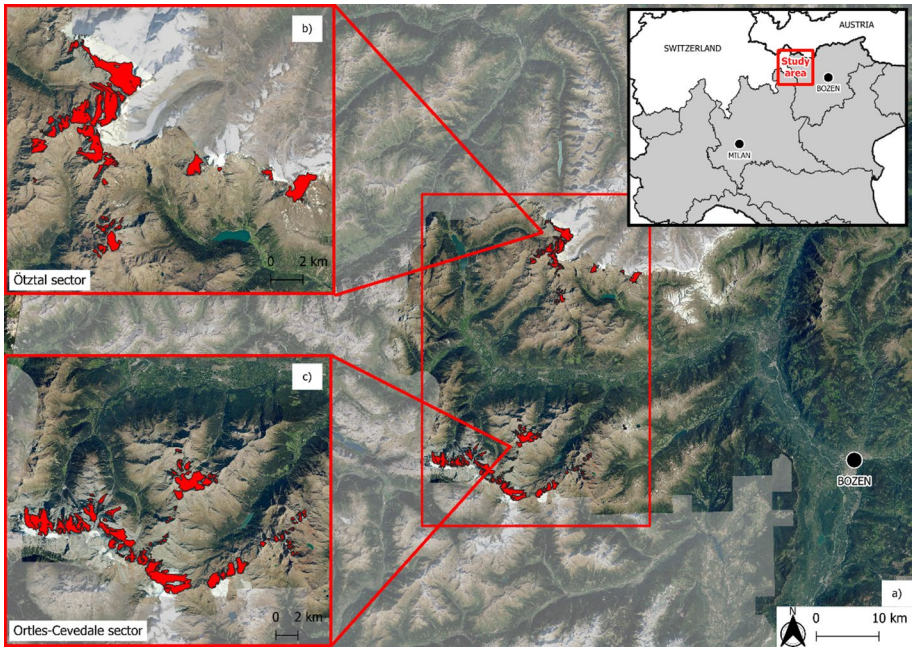

Fig. 2 **a** overview of the study region within the Alps; **b**, **c** focus on the two sectors studied in this research, in red the glacier outlines in 2020

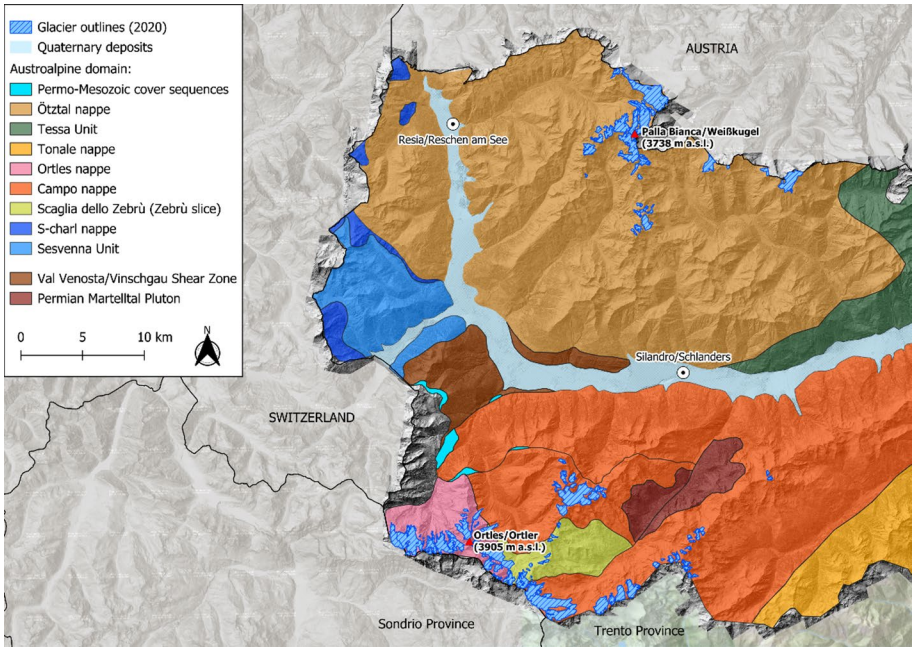

Fig. 3 Geological map of the study area

predominantly composed of metamorphic lithologies of the Austroalpine domain, while the Penninic domain outcrops in the northeastern sector [32]. The two areas of study, located in the western portion of the region, have dominant lithologies of Variscan metamorphic rocks characterized by polyphase deformation and metamorphism [33].

2 Data

To digitize glaciers and slope instabilities, we used aerial orthophotos and a digital surface model (DSM) from the Bolzano Province. The orthophoto was acquired on 12 October 2020 at a 20 cm spatial resolution and shows no cloud coverage. It is available on the Bolzano province geoportal (GeoCatalogo (buergernetz.bz.it)). To accurately detect the outlines of the glaciers, particularly in the debris-covered portions, the mapping was conducted with support from an interferometric coherence map derived from Synthetic Aperture Radar (SAR) data produced by [34] and created from Sentinel-1 data acquired during the summers of 2015–2017. Morphological information was retrieved from the 2016 DSM available on the Bolzano province geoportal. The DSM was generated from aerial photogrammetry and has a resolution of 0.5 m. We also supported the research with Google Earth imagery, which provides 3D views acquired between 2000 and 2020. The reconstruction of glacier area evolution was conducted, starting from the outlines published in the geoportal of Bolzano province for 1997, 2005, and 2017 [35]. Additionally, for analyses of the relationship between deglaciation and rockfall occurrence, we used the Little Ice Age (LIA) outlines [36]; the 2020 outlines were developed as part of this study. Geological and lithological data were obtained from the Swiss geoportal (www.geocat.ch), which provides datasets that also cover several Italian valleys located near the national border.

The tracks of the alpine routes used to assess the presence of intersecting rockfalls were retrieved from the geoportal of Bolzano Province (https://mapviegeoportalw.civis.bz.it/).

3 Methodology

3.1 Glacier outline mapping

The inventory update was carried out in QGIS (version 3.42.3) through manual digitalization of glacier outlines, based on knowledge of basic glaciological concepts and structures (e.g., crevasses indicating the presence of ice beneath debris-covered parts of glaciers, and the position of the proglacial stream).

On the one hand, manual digitalization of glaciers allows achieving a high level of accuracy, especially when using a basemap orthophoto at 20 cm spatial resolution. On the other hand, there are limitations when mapping the outlines of debris-covered portions. In this latter case, when working only with images in the visible range, it is not straightforward to identify if there is ice under the debris; secondary structures like crevasses can support during the assessment, but only if they are visible or recognizable. For these reasons, the digitization of glacier outlines was conducted using an interferometric coherence map derived from Sentinel-1 SAR (Synthetic Aperture Radar), thereby increasing the accuracy of outline delineation. InSAR can detect ground displacement between the acquisition of two or more images. Since glaciers, even when debris-covered, are subject to flow, this approach was applied to define the outlines of debris-covered portions. InSAR coherence, which measures the correlation between two SAR images, was considered as a proxy. Values range from 0 (no coherence) to 1 (high coherence). Low coherence indicates decorrelation, which may result from surface changes or movement, such as glacier flow. Higher values, on the other hand, indicate stable areas less affected by displacement.

The InSAR raster layer was imported into QGIS and overlaid with the 2020 orthophoto for a visual investigation of the glaciers. Based on this visual assessment and aligned with other studies [37], we created a coherence mask, setting the threshold to 0.62 and assuming that lower values correspond to areas subject to movement. From this coherence layer, we were able to define the extension of debris-covered glacier portions (e.g., Solda Glacier/Suldenferner or Madriccio Glacier/Madritschferner).

By combining the interpretation of the orthophoto and the InSAR map, we compiled an updated inventory of glacier outlines in our study region. The glaciers were first digitized, creating two polygonal shapefiles, one for each sector considered. Later, the attribute tables were checked and homogenized, allowing the merging of the shapefiles into a single one to facilitate data management. The attributes associated with the 2020 outlines are reported in Table 1.

The names of the glaciers were retrieved from the inventories of preceding years. Due to the retreat of some glaciers, we had to create new polygons. For these, we decided to keep the main glacier name, followed by an indication of location or dimension (e.g., the main glacier name + “superior” or the main glacier name + “niche”).

The morphological classification is based on the GLIMS guidance (www.glims.org), but in some cases, the terminology has been adapted to better describe the new morphology developed by the glacier under substantial shrinkage. The area was expressed in km^2 and computed in QGIS. The aspect values represent the mean orientation of each glacier with respect to north. These statistics were calculated in R-Studio as the arctangent of the respective mean values of the sine and cosine grids of terrain aspect. The resulting angle was then converted into the corresponding cardinal point.

Table 1 Attributes associated with each glacier in the inventory

Attribute	Description
Name	Glacier name
Sector	Ortles-Cevedale or Ötztal
Category	Valley or mountainous
Snout conditions	Debris free or Debris covered
Morphology	Classification of the glacier morphology (e.g., cirque, niche)
Notes	Additional information
Valley	Name of the valley
Mean slope	in degrees (°)
Max slope	in degrees (°)
Mean aspect	As cardinal points
Area	Km^2
Polygon ID	Number
Glacier ID	Number

Using these polygons, we reconstructed the area evolution from the end of the LIA to 2020. More precisely, this analysis was conducted across two time windows: (I) an overview from the LIA to 2020 to capture the overall evolution across the farthest available dates, and (II) a more recent reconstruction from 1997 to 2020 to provide insights into the rapid disaggregation of recent years. The LIA polygons were retrieved by [36] and represent the extension reached at the end of the period (around 1850). Their reconstruction is based on field evidence, historical topographic maps, DEMs, and orthophotos. The glacier boundaries representing the extent in 1997, 2005, and 2017 are produced by [35]. As explained by the authors, the polygons for these years were created with two approaches: (I) directly, from optical data, or (II) indirectly, assessing the presence of crevasses in debris-covered areas or by interpreting the results of the difference of DEMs that produced mass losses not caused by erosional processes.

3.2 Slope instabilities mapping

The main analyses were conducted using QGIS (version 3.42.3), SAGA GIS (version 7.8.2), and RStudio (version 2024.12.1). The identification of slope instability events was conducted by analysing the 2020 orthophotography to provide an initial assessment of debris on the ice surface. To refine the delineation of the detachments, precise insights were obtained from the DSM and the Google Earth 3D viewer, which were particularly helpful for identifying detachment zones and scars.

We defined two classes to describe the slope instabilities based on their morphology: rockfalls and side wall debris (Fig. 4a-b). We categorized events as "Rockfalls" if they had:

- Clear lobate shape in the accumulation zone.
- Visible single detachment zone and visible scar on the mountainside.

"Side wall debris" class includes all those events where:

- The debris is sparse at the toe of a side.
- There is an unclear or indistinct detachment zone, often with no visible scars on the slope, typically due to multiple small-scale falls from the same mountain area. These deposits are most likely the result of widespread weathering and erosion processes that have affected the deglaciated rock wall.

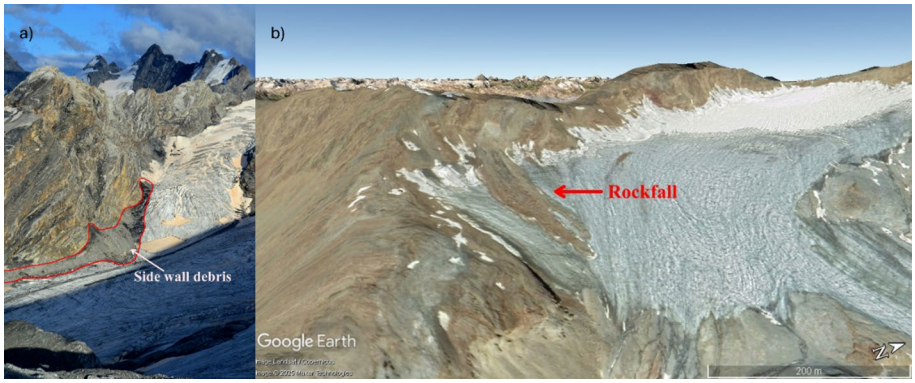

Fig. 4 **a** Side wall debris in the Ortles-Cevedale sector (photo taken in August 2024 by M. Di Biase); **b** example of rockfall in the Ötztal sector (image acquired in 2019, Google Earth)

Table 2 Attributes of the slope instabilities

Attribute	Description
Class	Rockfall or Side wall debris
Sector	Ortles-Cevedale or Ötztal
Valley	Name of the valley
Slope	Average slope of the polygon. Expressed in degrees (°)
Aspect	As cardinal points
Area	In Km^2
Geology	Information about the geology and lithology
Morphology of the glacier	Morphology of the glacier on which it was deposited

Table 3 Additional attributes for instabilities classified as "rockfall"

Attribute	Description
Maximum and minimum elevation	Height of the scarp top and of the distal end
L	Horizontal travel distance
H	Heigh drop
Heim's Ratio	H / L
Fahrböschung	As the angle between H and L

The attributes associated with all slope instabilities are reported in Table 2.

For those classified as "Rockfall" we retrieved additional morphometric attributes reported in Table 3. The minimum, maximum and mean elevations were computed in R-Studio by overlapping the rockfall polygons on the DSM; the minimum elevation is computed as the lower altitude of the deposition zone, the maximum one represents the highest altitude of the detachment zone, and the mean elevation represents the mean altitude of each displacement. In addition, for all rockfalls in each sector, we computed the average maximum elevation to analyse the altitude distribution of the detachment zones. We also calculated indices characterizing rockfall mobility, namely Heim's Ratio and the Fahrböschung angle [38, 39]. A more detailed description of the methodology used to retrieve these values is provided in the following paragraph.

3.3 Runout evaluation and modelling

The runout is the distance the material dragged by a landslide travels. Quantifying its extension contributes to the definition of vulnerable areas. In this study, we assessed

the mobility of rockfalls based on two approaches commonly applied in the literature: Heim's ratio and the Fahrböschung angle.

The Heim's ratio [38] is computed as the ratio between *H/L* (Fig. 5a), where H (Height drop) represents the vertical distance between the highest point and the lowest point of the fall; L is the horizontal distance of the rockfall, namely the projection on the plane between the highest point and the lowest point. Heim's ratio, also known as "apparent friction," is used as a proxy for the friction coefficient of landslides [39, 40]. This coefficient, first postulated by Heim, expresses the idea that the travel distance of a rockfall material depends on the height of the fall, on the conditions of the pathway, and on the size of the blocks. According to [40], long runout is considered to occur when Heim's ratio is < 1.0, whereas less energetic events have Heim's ratio > 1.0.

The relation between H and L is not studied only in the form of a ratio, but also as the angle between these two components, and it is referred to as "Fahrböschung" (Fig. 5b) [39]. The equation for calculating the Fahrböschung angle is (Eq. 1):

$$\phi = \tan^{-1}(H/L) \tag{1}$$

Larger landslides tend to produce lower Fahrböschung angles than smaller detachment events. Still, it is important to consider that the runout length is not controlled only by the dimension of the fall, but also by (I) the impact pressure and the shear rate on the ground; (II) initial failure volume, and (III) topography [40–42].

Additionally, regarding the Fahrböschung, it can be stated that the lower the angle, the higher the mobility of the flow [39]. According to previous studies [43], the horizontal displacement is not primarily controlled by the height drop but by the volume of the rockfall. Since we did not have any volume data, we built the correlation using rockfall area to test the relationship between the horizontal and rockfall dimensions. We acknowledge the limitations of this approach; nevertheless, we refer to the relationship reported in [44], which indicates that the volume-to-surface-area ratio follows a power law with an exponent of approximately 1.4. Based on this theory and given that it is the only model available for our analyses, considering the large area of interest and the

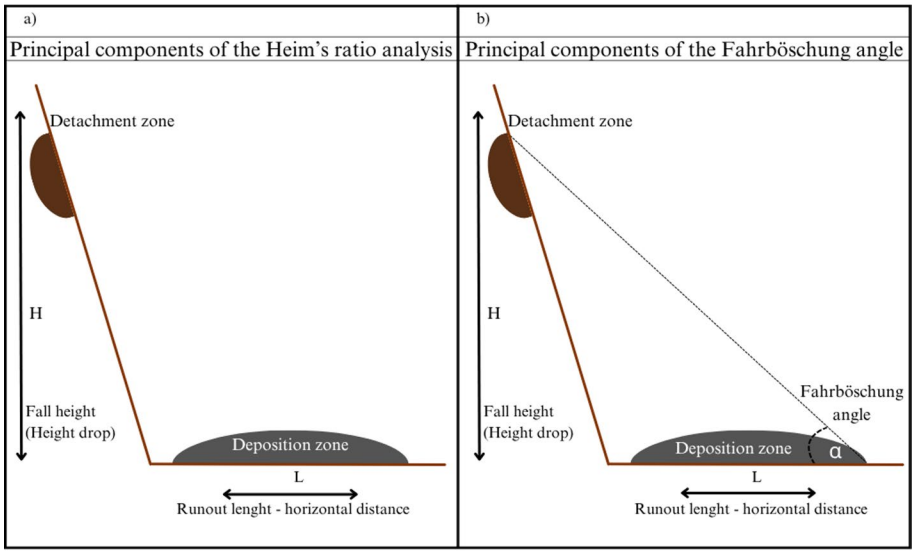

Fig. 5 **a** schematic representation of the components involved in the computation of Heim's ratio; **b** schematic representation of the Fahrböschung angle

limited availability of historical DSM data, we computed the correlation between horizontal displacement and rockfall dimension.

When analyzing runout, it is important to consider that its variability is partly influenced by the frontal position of the deposits. As a result, runout reflects the combined effects of rock mass, the translation, and the spread. These dynamics are especially pronounced on glaciers, where debris movement is also affected by ice flow. The additional travel distance due to spreading can have a profound effect on the runout, especially when the effective basal friction is low [45].

Starting from the measured elevation and angle values retrieved from the instabilities mapped in the 2020 orthophoto, we modeled potential runout distances and paths by assuming different friction parameters; this allowed us to observe changes in debris distribution across the glaciers and assess their locations relative to alpine routes. The simulations were performed using the Gravitational Process Path (GPP) tool in SAGA GIS [46]. We simulated three scenarios assuming three different friction parameters based on previous literature studies and tests, as we did not have field data to calibrate these values. The friction values used in GPP are:

- low friction = 0.2; considered as the extreme situation. It is the lowest friction value reported for samples related to rock-ice avalanche events in the Swiss Alps [47].
- medium friction = 0.4 is the friction derived from Heim's Ratio. To retrieve this value, we first removed outliers from Heim's ratio results using the Interquartile Range method, then averaged the minimum values for each sector.
- high friction = 0.65 was retrieved by [39] from experiments; here it is used as an upper boundary.

The GPP tool in SAGA GIS allows for setting different parameters to calibrate the model with the best-fitting values to describe various landslide types and dynamics [46, 48, 49].

The input parameters are the DEM of the area under investigation and an integer raster that encodes the positions of the detachment areas using their unique IDs. The process path was modelled using "random walk" trajectories, which compute the path using a grid-based random walk. With this approach, all lower-elevation neighbours of a central cell in a 3×3 window are potential flow path cells. To improve this sample and calibrate it to different geomorphologies, it is possible to provide additional specific parameters, such as a slope threshold and a persistence factor that describes divergent flow. From each starting point, various random walks are elaborated based on the Monte Carlo simulation; each run generates a slightly different process path.

To simulate the runout, we adopted the "1-parameter friction model" originally proposed by [50] and later reviewed by [48, 51]. We selected "rolling" as the primary mode of motion, although we acknowledge that, especially on gentle slopes or glacial surfaces, the actual motion may involve a combination of rolling and sliding.

The particle velocity is then calculated for each cell in the DEM. For any two adjacent cells, where one has a lower elevation, it is possible to construct a triangle using the vertical and horizontal distances between their centroids as the legs (Fig. 6). The particle's velocity is then computed along the profile line, which corresponds to the hypotenuse of the triangle.

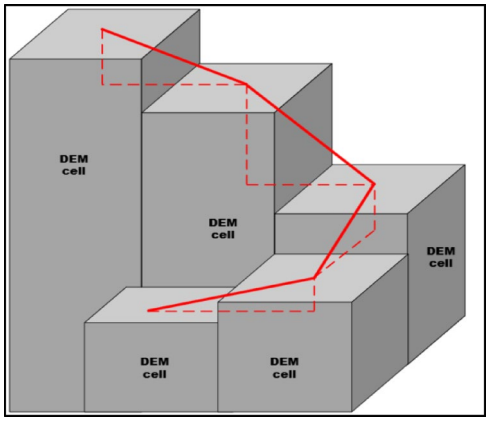

Fig. 6 Schematic representation of the flow path along the triangles built in the "1-parameter friction model" (Authors' adaptation from [49])

The cells touched by this line are delineated with the random walk model, and the velocity in each position is controlled by the velocity in the previous cell of the path. The area between the source and the point where the velocity becomes 0 is the runout area, i.e., the area covered by the rockfall deposit [49]. The result is a "process area" raster that describes the extent of a landslide deposit and the frequency with which a cell participates in a process; in other words, it quantifies how likely a cell is to collect material from rockfalls or other phenomena.

3.4 Relationship between rockfalls and alpine paths

Once we extracted the potential run-out paths in SAGA, we analysed the spatial distribution of rockfalls over the mapped glaciers to identify areas more prone to destabilization and to evaluate the number of intersections between debris deposits and alpine tracks, where present. The shapefiles of the alpine tracks were retrieved from the official geoportal of Bolzano Province (GeoCatalogo (buergernetz.bz.it)) and imported into QGIS. We clipped the routes within the 2020 glacier outlines and excluded all trails outside the glaciated areas from the analyses. We refer to the crossing points as "perfect intersection" when no buffer is considered between the trails and the rockfall deposit. In case a polygon is crossed by a trail multiple times, each intersection is counted independently.

4 Results

4.1 Glacier recession

Reconstruction of the glacier area over the years confirms the rapid disaggregation of glaciers in the Alps. Glaciers in our study region suffered a strong area contraction, i.e., -69.44% of area between the end of the LIA and 2020 (Figs. 7a, b and 8).

The retreat rates were remarkably rapid in recent years; between 1997 and 2020, glaciers in the study area lost 38% of their area in the Ortles-Cevedale group and 38.9% in the Ötztal group. In the Ortles-Cevedale group in 2020, we mapped a total area of 29.2 Km^2, of which 24.7 Km^2 are debris-free and 4.5 Km^2 are covered by debris. Concerning the Ötztal group, the total glacier area in 2020 was 15.97 Km^2, of which 14.29 Km^2 are debris-free and the remaining 1.68 Km^2 are debris-covered. In the Ortles-Cevedale group, glaciers facing south saw higher percentages of annual retreat (-4.35% /yr), and

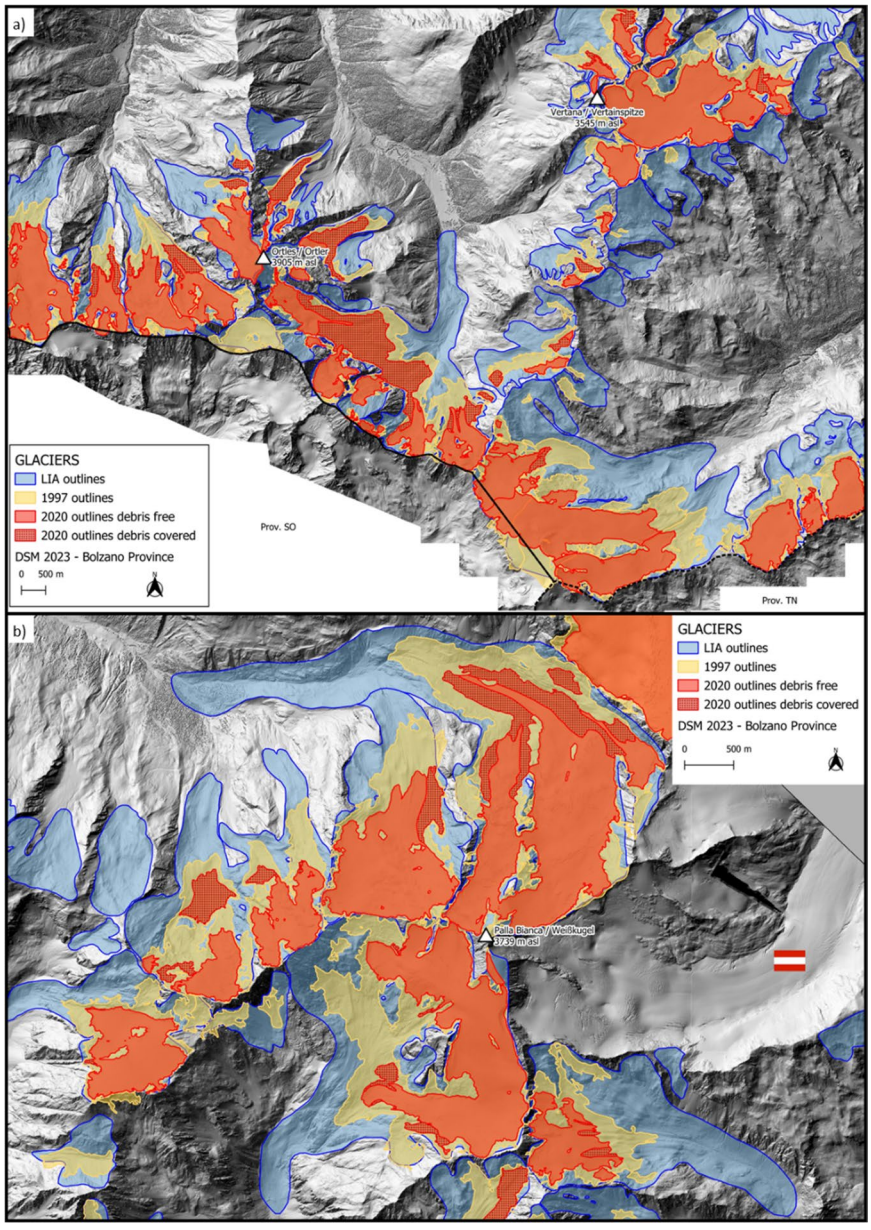

Fig. 7 Maps showing the evolution of the glacier area in the study region since the LIA – **a** the Ortles-Cevedale sector; **b** the Ötztal group

in the Ötztal sector, the situation was more heterogeneous, with higher percentages of annual loss on glaciers facing NE (-2.66%/yr) and S (-2.3%/yr) (Fig. 9).

4.2 Inventory of the slope instabilities

In our study region, we identified 500 slope instabilities with deposition zones on the glaciers (Fig. 10).

With reference to slope instabilities in the Ortles-Cevedale group, we mapped a total of 230 events (63 sidewall debris and 167 rockfalls). These events are predominantly exposed to the west and the northeast (Fig. 11a), with 20% for each sector. A significant portion also faces the east (E) and northwest (NW), accounting for 16% and 19% respectively. Southeastern (SE) and southern (S) exposures are less common, accounting for

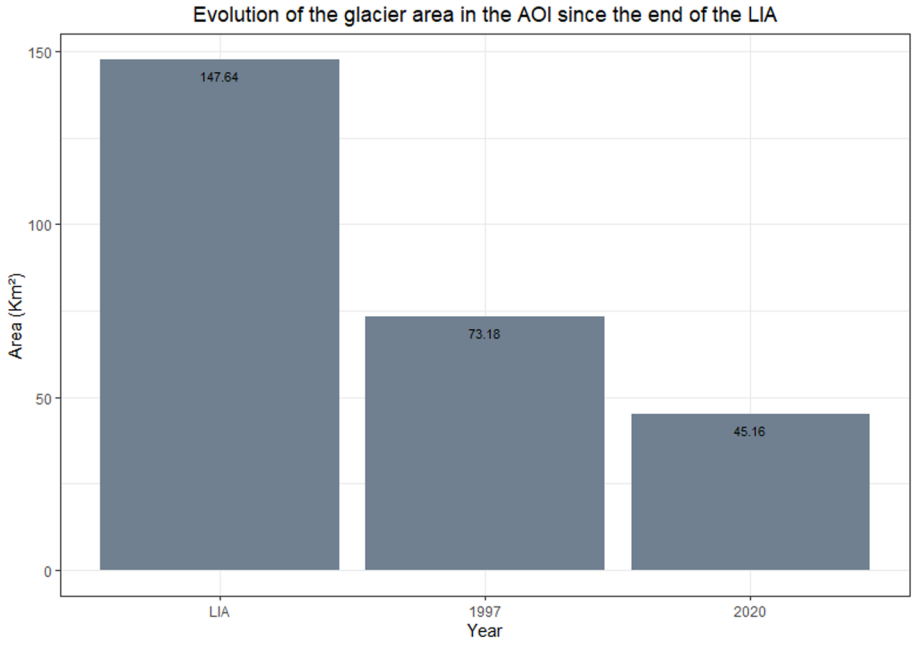

Fig. 8 Evolution of the glacier area in the entire study region since the LIA

8.6% and 8.2% of the events, respectively. Southwest (SW) exposures account for 6.5%, while northern (N) exposures are the least frequent, with only three events, corresponding to 1.3% of the total. Analysing the events distribution per geological units in this sector, we observe that: 145 detached within the Campo nappe, 34 within the Zebrù slice and the remaining 51 occurred in the Ortles nappe. The involved lithologies are mainly quartz phyllites (about 57% of the mapped landslides) and gneiss (about 13%). Sedimentary rocks such as dolomites and limestones are also involved (about 28%). Fewer phenomena (about 2%) occur in local amphibolite veins.

In the Ötztal sector, we identified 270 events, of which 142 were classified as rockfalls. In this sector, we observe a high frequency of detachments exposed NW (70 events), representing 25.93% of the total. The percentages of mapped phenomena in the other sectors are: 17.78% E, 17.04% W, 13.3% SW, 11.85% NE, 8.15% SE, 5.19% S, and less than 1% facing N (Fig. 11b). For what concern the geology, all the slope instabilities in this sector, occurred within the Ötztal nappe in gneiss and quartz phyllite.

For events classified as "rockfalls", we conducted additional analyses, assuming that this category allows for a more complete morphological description. Regarding the frequency, glaciers in the Solda Valley (Ortles-Cevedale) and Valle Lunga (Ötztal) are the most affected, with 76 (33%) and 117 (43.3%) phenomena, respectively. To better understand this relation, it is necessary to compare these data with the number of glaciers in each valley, noting that a higher number of glaciers in a valley suggests a higher probability of paraglacial instability events. Additionally, this approach is not sufficient to describe event occurrence, as other parameters, such as aspect or runout, also need to be considered to quantify a valley's vulnerability.

Concerning the distribution of rockfalls in the Ortles-Cevedale sector, their detachment zone is located between 2922 m a.s.l. and 3765 m a.s.l.; rockfalls have a mean detachment altitude of 3271 m a.s.l. and are more frequent in the range between 3300 and 3350 m a.s.l. (Fig. 12).

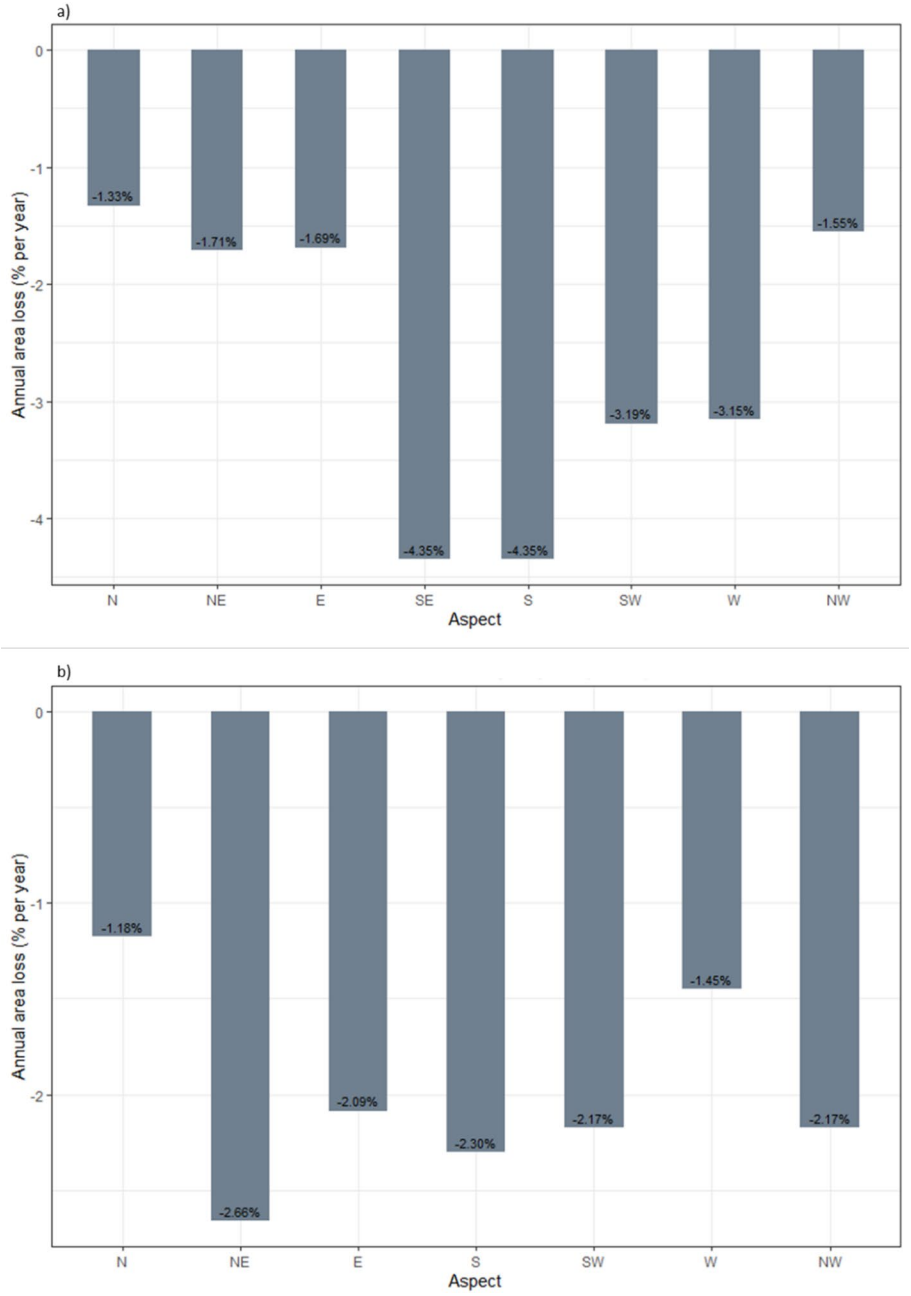

Fig. 9 **a** Mean annual loss (in %) per aspect – Ortles-Cevedale sector; **b** Mean annual loss (in %) per aspect - Ötztal sector

If we consider their distribution per aspect, the detachment zone of NW rockfalls is located at a lower elevation, with a mean of 3184 m a.s.l.; in contrast, source areas facing SE feature a higher altitude for their detachment niche, with a mean of 3316 m a.s.l. In this sector, the mean slope of the rockfalls is 37.32°, the detachment point (with 1 m buffer) has a mean slope of 66.72°, and 73.62% of the niches have a slope higher than 40° (often assumed as a reference to describe potential rockfall sources [52]). In the Ötztal group, the mean detachment elevation is 3309 m a.s.l., and detachment zones are more frequent between 3300 m a.s.l. and 3350 m a.s.l. In general, the distribution of detachment zones is between 2950 m a.s.l. and 3650 m a.s.l. (Fig. 13). In this sector, rockfalls

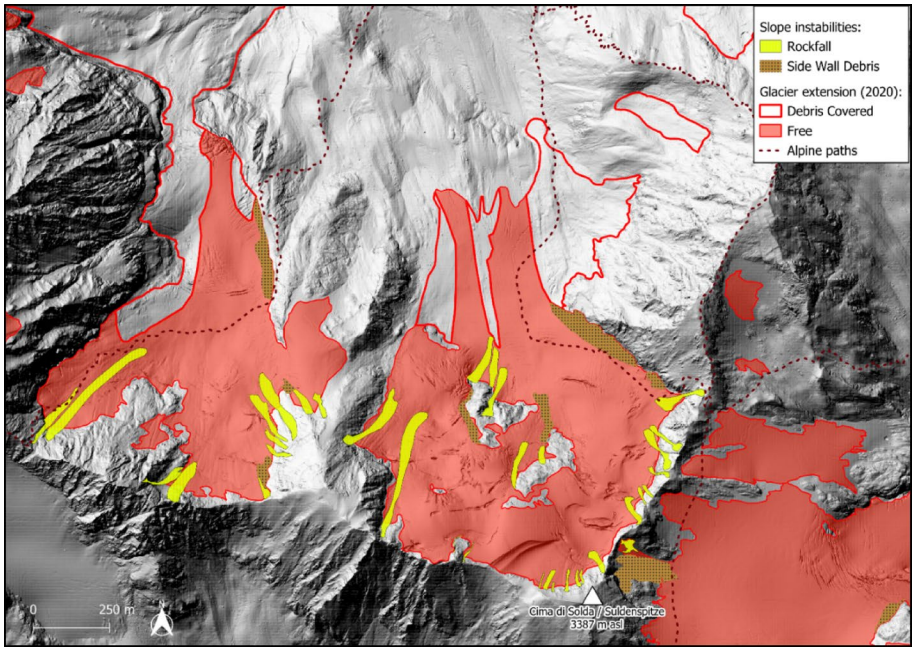

Fig. 10 Example map of the slope instabilities that occurred over the Solda glacier in the Ortles-Cevedale massif

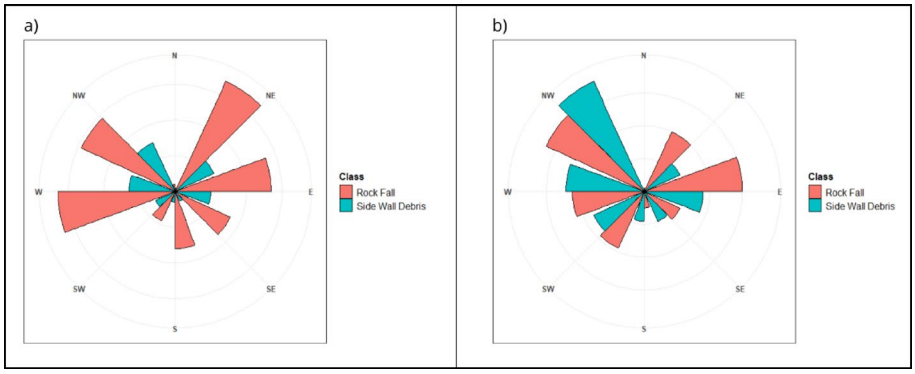

Fig. 11 Slope instabilities distribution per aspect; **a** Ortles-Cevedale sector, **b** Ötztal sector

facing NE have the lowest detachment elevation; in contrast, rockfalls facing SW have the highest detachment elevation (Fig. 14). In the Ötztal group, the mean slope is 37.52°. Considering a 1 m buffer around the detachment niches, we found a mean slope of the detachment portion to be 61.37°, and 74.22% of the niches have a slope greater than 40°.

Due to the incomplete data available, it was not possible to define a precise date or period for each event. However, by considering the source location with respect to the glacier outlines, it was possible to provide a general indication of the timing of each event.

In the Ortles-Cevedale:

- 106 / 167 rockfalls (63.4%) are within the LIA outlines.
- 34 / 167 rockfalls (20.35%) are within the 1997 outlines.
- The remaining 27 (16.16%) polygons have source locations that exceed the available outlines.

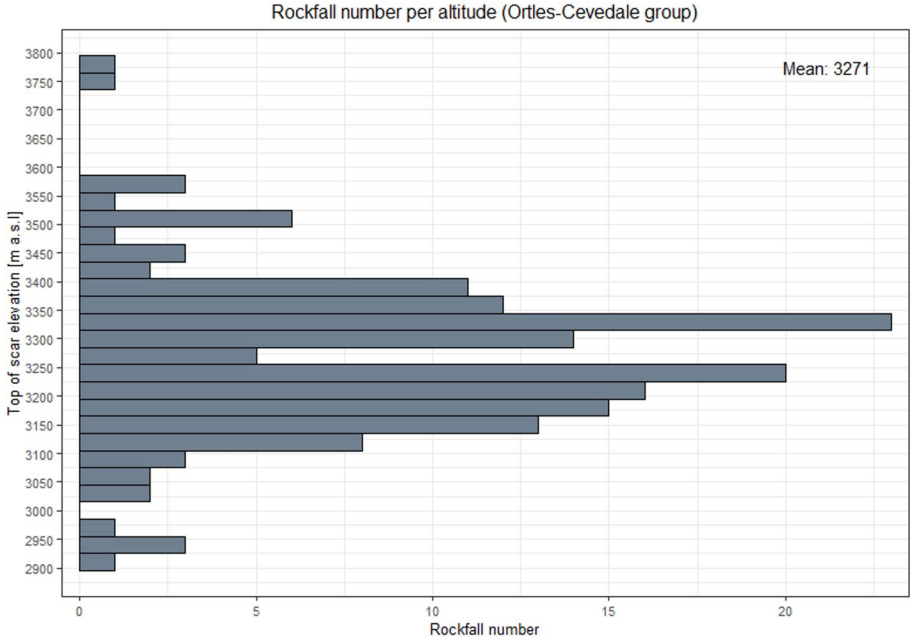

Fig. 12 Rockfall distribution per elevation in the Ortles-Cevedale sector

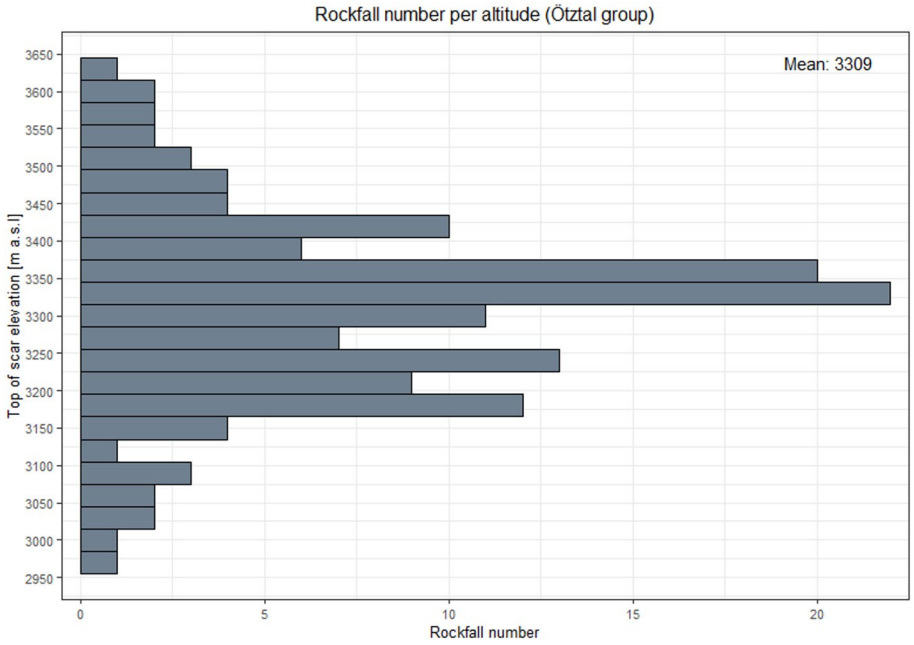

Fig. 13 Rockfall distribution per elevation in the Ötztal sector

As far as the Ötztal sector is concerned:

- 69 / 142 rockfalls (48.6%) are within the LIA outlines.
- 29 / 142 rockfalls (20.4%) are within the 1997 outlines.
- The other 44 polygons (31%) have their detachment zones outside the glacier polygons considered in this study.

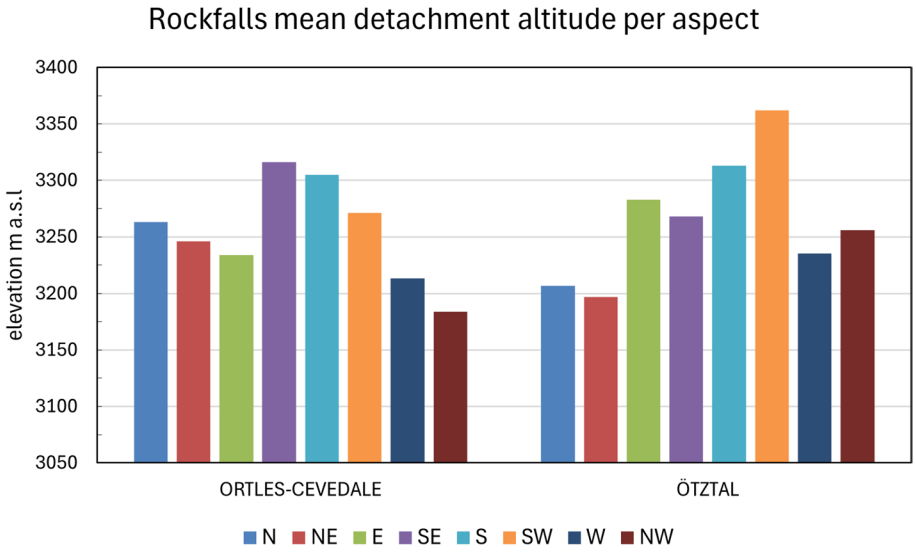

Fig. 14 Average rockfall detachment elevation distributed per aspect for the two mountain sectors

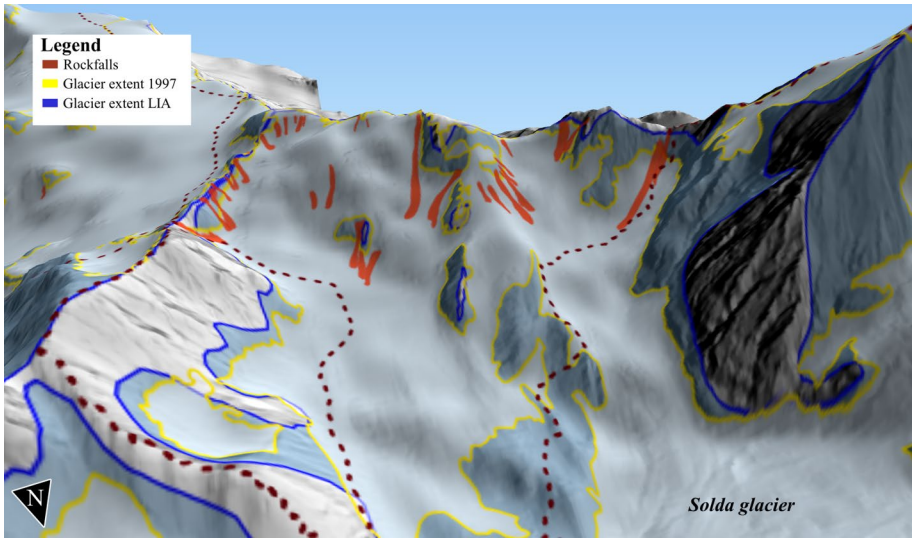

Fig. 15 Example of rockfalls with a detachment zone within the LIA outlines

We hypothesize that if the detachment zones are within the LIA outlines, their detachment occurred after the post-LIA deglaciation (post-1850), based on the outlines available from [36]). If the detachment is within the 1997 outlines (Fig. 15), it indicates that the rockfall detached between 1997 and 2020. We hypothesize that rockfalls with detachment zones outside the glacier outlines occurred without a strict relationship to glacial evolution, but may have been influenced by permafrost degradation, weather-related degradation, or a delay in the paraglacial response [53, 54].

With reference to the 2020 orthophoto, in the Ortles-Cevedale sector we were able to count a total of 12 perfect intersections with alpine paths (eight with rockfalls and four with side wall debris) (Fig. 16). Considering the most frequent mean aspects of these 12 instabilities, we can observe that four of them are facing NE, three are facing W and the other five events are negligible in this statistic. In the Ötztal group, we observe only two

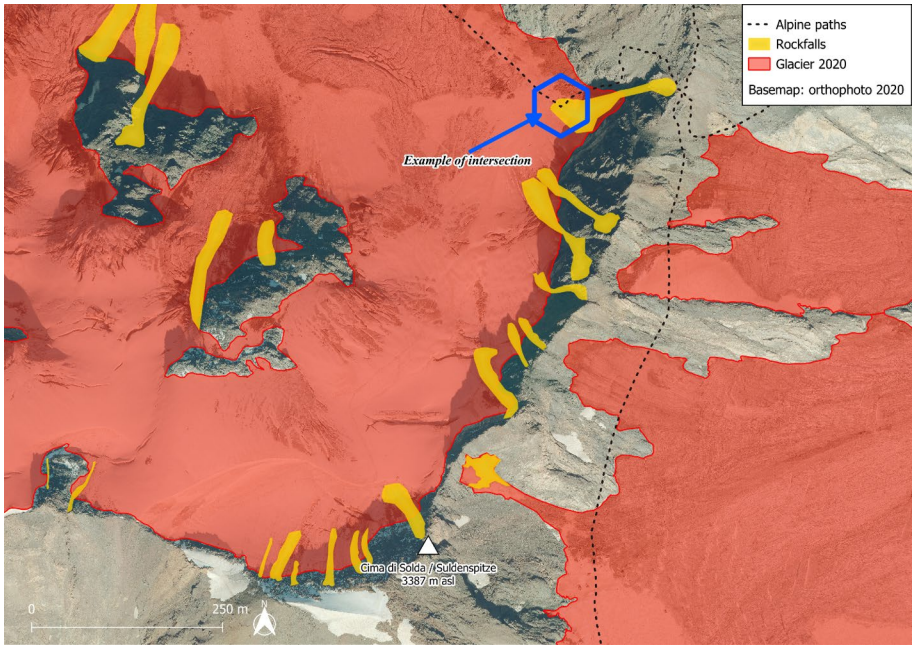

Fig. 16 Example of intersection between rockfalls and an alpine path in the Ortles-Cevedale group

perfect intersections; this is explained by the fact that fewer alpine routes cross the glaciers in this sector.

4.3 Runout assessment

The runout assessment was completed with the analyses of Heim's ratio and the Fahrböschung angle [38, 39].

The average Heim's ratio, which is expressed as the ratio between the components H and L of a landslide, is 0.86 in the Ortles-Cevedale group and 0.87 in the Ötztal sector. In the Ortles-Cevedale sector, 33 / 167 rockfalls have a Heim's ratio > 1.0, and thus, according to [40], can be classified as rockfalls with short runout, while the remaining 134 rockfalls are long-runout events. As far as the Ötztal rockfalls are concerned, 35 / 142 have a Heim's ratio > 1.0; therefore, we have 107 long runout events.

In the Ortles-Cevedale sector, we found an average Fahrböschung angle of 40.25° supported by a very strong Pearson correlation between H and L ($r = 0.96$). In the Ötztal sector, the mean Fahrböschung is 40.16° with a Pearson correlation between H and L resulting in $r = 0.89$. These correlations (Fig. 17) suggest that rockfalls with higher vertical difference tend to displace debris over longer distances.

As previously explained, we did not have volume data; therefore, to quantify the role of rockfall dimension over L, we structured the correlation using area (Km^2) as an indicator of volume [44]. These correlations exhibit strong Pearson values, with $r = 0.76$ in the Ortles-Cevedale and $r = 0.81$ in the Ötztal, indicating that small detachments tend to produce shorter runouts.

Furthermore, these correlations confirm the hypothesis of [44], who found a scale between Fahrböschung results and rockfall dimensions.

Regarding the GPP simulation, the results are presented in Tables 4 and 5, and visual differences are evident in Fig. 18.

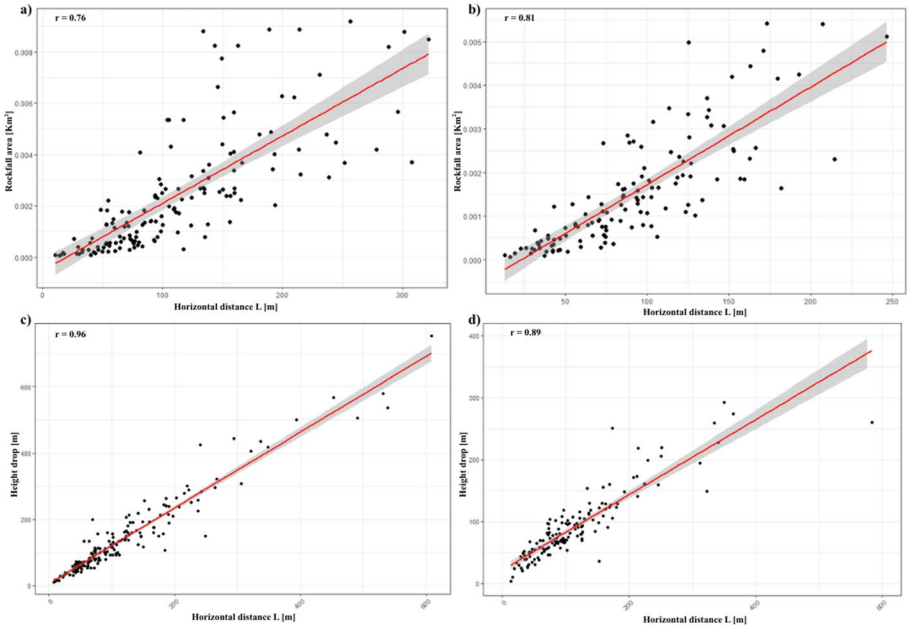

Fig. 17 **a** Pearson correlation between rockfall area (Km^2) and L (Horizontal distance) for the rockfalls in the Ortles-Cevedale sector; **b** Pearson correlation between rockfall area (Km^2) and L (Horizontal distance) for the rockfalls in the Ötztal sector; **c** scatterplot between rockfall H (height drop) and L (Horizontal distance) for the rockfalls in the Ortles-Cevedale sector; **d** scatterplot between rockfall H (height drop) and L (Horizontal distance) for the rockfalls in the Ötztal sector

Table 4 Summary of the results from the GPP simulation in the Ortles-Cevedale sector

Ortles – cevedale sector	
Friction value	**Number of intersections**
High friction scenario (0.65 μ)	11
Medium friction scenario (0.4 μ)	18
Low friction scenario (0.2 μ)	21

Table 5 Summary of the results from the GPP simulation in the Ötztal group

Ötztal sector	
Friction value	**Number of intersections**
High friction scenario (0.65 μ)	2
Medium friction scenario (0.4 μ)	8
Low friction scenario (0.2 μ)	10

According to these simulations, the high-friction scenario best aligns with the observed situation in the 2020 orthophoto. The bias between this outcome and the medium value retrieved from the actual situation is due to the lack of additional field data to apply in the GPP model, which would have improved calibration. Nevertheless, the GPP simulation results demonstrate the heterogeneity of possible runouts, confirming that low-friction events pose a higher risk to alpine infrastructure. The long runout generated by these low-friction events is driven not only by the amount of material but also by its typology (e.g., rock-ice avalanche, as in [47]) and by the condition of the substrate.

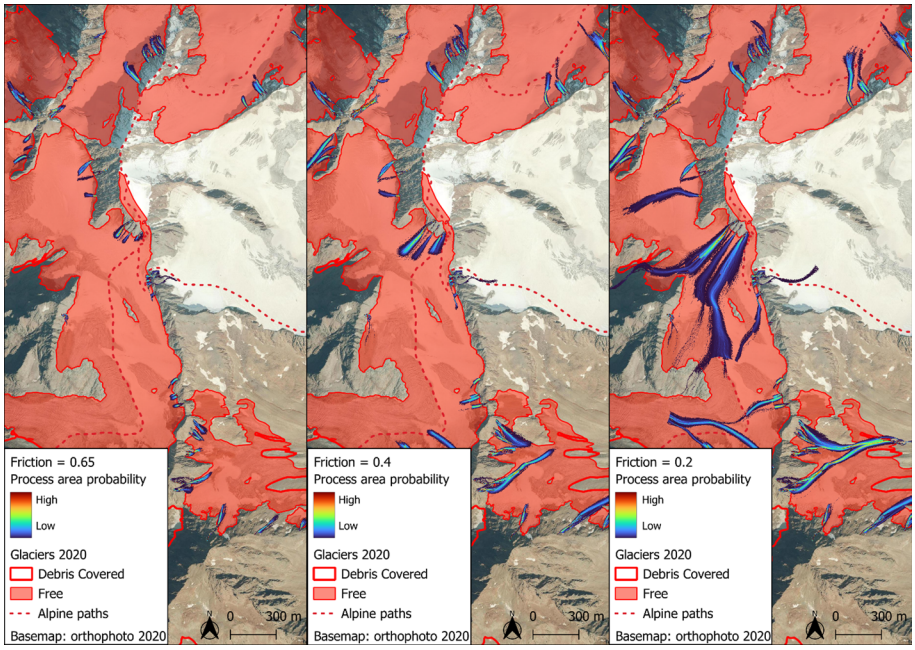

Fig. 18 results of GPP runout simulation using 3 different friction values, zoom in on the Ötztal group

5 Discussion

Through this research, we confirmed the ongoing rapid disaggregation of glaciers in the study area (-69.44% of area between the end of the LIA and 2020). Additionally, we assessed glacier changes over a shorter time window (1997–2020), demonstrating clearly visible changes within an average lifetime, as glaciers in both our sectors lost ~38% of their area over this period. Our glacier inventory classifies the surface, distinguishing between debris-covered and debris-free portions. It is recommended that this distinction be maintained in future inventories, as it will enable us to assess how retreat rates differ in the two situations.

As a consequence of this glacier retreat, portions of mountains previously covered and supported by ice become exposed, leading to changes in temperature, stress fields in the rocks, and mechanical and thermal erosion [55–56–57].

We investigated the distribution of slope instabilities in our study region, providing the first inventory of all events that occurred until 2020. Previous studies (e.g. [58, 59]), have emphasized the importance of rockfall inventories as key input factors for analysing not only the distribution but also the triggering and predisposing factors of such events, to develop effective risk management strategies. Our inventory aligns with this necessity; it is the first dataset for the Venosta Valley, compiled without discrimination by size or typology. The obtained results align with the hypothesis that slope instabilities may be linked to the rapid deglaciation currently occurring [14, 22, 23, 59].

Mapping slope instabilities using a high-resolution orthophoto enabled the collection of a precise set of all events, avoiding discrimination based on size, volume, and epoch that would have been necessary with a geodetic methodology. From the digitization of rockfall bodies, we were able to retrieve valuable information to characterize the events in terms of geometry, and their temporal relation to deglaciation. We recognize that lithology plays a major role in controlling the initiation of rockfalls; however, we do not investigate this aspect in detail because information on the slope-scale structural

setting, which strongly influences the fracture network and slope stability, is lacking. As explained by [40], the apparent coefficient of friction (Heim's ratio) manifests some limits: (I) L does not strongly depend on H but more on the volume, and (II) it is based on the idea that the energy released during the fall is constant. If so, we can conclude that Heim's ratio and the Fahrböschung are parameters helpful to compare the mobility of different landslides using a homogeneous measure, but it is not correct to interpret only these parameters in risk assessment analyses based on the rockfall mobility.

We are aware that the dating of the rockfalls is not accurate year to year; however, given that we worked solely with open data, this was the only applicable approach to relate the events to the deglaciation periods. Further studies could provide a dating of the events based on different satellite images acquired over the last 30 years, allowing for the reconstruction of their presence. However, apart from the time-consuming methodology, only rockfalls visible at the satellite image resolution (10–30 m) would be dated. Alternatively, it is possible to use high-resolution historical images; in such a case, the problem is posed not only by the uncertain availability of images, but also by their "on request" accessibility.

It is not straightforward to compare our findings with those of previous similar studies because some parameters are influenced by regional differences, such as geology, altitude range, and glacier evolution. Regarding the rockfall exposition, our study aligns with that of [25], which found that N-facing slopes exhibit lower scarps, while S-facing slopes exhibit niches at higher altitudes. Considering that we do not have a precise indication of the detachment epoch to correlate with the deglaciation rates, we can only offer some hypotheses to explain this distribution. The first hypothesis relates the instabilities to the post-glacial debuttressing phenomenon; it is indeed possible that north-facing faces deglaciated recently compared to south-facing slopes; therefore, these northern slopes would be currently readjusting to a post-glacial situation through slope instabilities distributed at high altitudes, because the lower portions deglaciated previously and have already released the stress after the deglaciation. The second hypothesis relates to the influence of permafrost on high-altitude rockfalls; indeed, it is also possible that the rockfall distribution is conditioned by fluctuations in local thermal regimes, daily solar radiation, or weathering that could enhance permafrost thaw and, therefore, slope stability.

The average altitude of the detachment points in our sector is significantly higher than the values found in other studies conducted in nearby sectors (ours is ~300 m higher) [25]; this is because in our region, the altitude range includes peaks reaching high altitudes between 3800 m a.s.l. and 3900 m a.s.l. (Palla Bianca and Ortles). Thus, the resulting mean detachment altitude is influenced by events that occur in these high portions.

Our study confirms the statistical relation found by [38] between the height drop (H) and the travel distance (L), in our case with Pearson correlation values close to 1 (r = 0.96 and 0.89), similar to what was found also in another study conducted in a nearby area [25]. Regarding this correlation [38], initially stated that L is mainly influenced by H; however [39], later proposed a positive correlation between L and landslide volume. The author emphasized that the positive correlation between H and L is not driven by the height drop but rather by landslide volume, explaining that larger landslides travel longer distances (L) downslope. Given that in our study we could not retrieve a precise indication of volume, it was not possible to test this second correlation between L and

volume; anyway, supported by the literature of the sector [44], we developed a valid correlation (r=∼1) assuming the rockfall area as an indication of the size.

We decided to analyse the relationship between H, L, and rockfall size in more detail, as we found Heim's ratio and Fahrböschung values slightly higher than those reported in other research in nearby sectors. We can explain our results accordingly by interpreting the values proposed by [39]. In their research, it is found that small rockfalls exhibit a higher coefficient of friction (around 0.6), whereas larger rockfalls exhibit a substantially lower coefficient (0.3). Observing Fig. 17, we can confirm [39]'s theory. Indeed, it is possible to notice a cluster of rockfalls around the lower values of area, suggesting that these events influence the computation of the average Heim's ratio in the two sectors, resulting in values ∼of 0.8. In addition, the correlations we built among H, L, and area demonstrated that there is also a significant interrelation between rockfall size, values of Heim's ratio, and Fahrböschung in our inventory.

Regarding the GPP runout model, we did not have any valid field data to calibrate the tool with local information. Therefore, we based our description on realistic parameters, which enabled us to produce a homogeneous description across the study region. More specific considerations would be required when focusing on single events.

The GPP model demonstrates that, potentially in the future, other falls may intersect alpine infrastructure or alpine routes. In this prediction, it is also important to consider that the runout depends on the friction coefficient, which varies with the type of instability (e.g., rockfall on ice or ice-rock avalanches). This is why we assumed three different friction scenarios. Indeed, we wanted to provide the broadest possible overview of the possible scenarios. As result we demonstrated that compared to the actual situation retrieved from the 2020 orthophoto, only in one of the three scenarios (high friction) the alpine paths are equally or slightly less exposed to intersections with rockfalls; the other two situations are helpful in underline that potentially alpine paths in our study region may be touched by slope instabilities increasing risks for human activities and consequences for alpinists.

6 Conclusions

We generated the first database of all instability events in the paraglacial environment of the Venosta Valley in Italy. To better understand the relationship between these instabilities and deglaciation, we also studied glacier evolution from the end of the LIA to 2020. As part of this research, we generated the 2020 outlines of the glaciers in this sector. With these results, we contribute to updating the archive of glacier outlines and attest to the rapid retreat of glaciers in this sector. The reconstruction of glacier evolution over the last century helps to understand their fundamental role as water resources for northeastern Italy; indeed, these glaciers feed the Adige River, one of the longest in the region, providing fresh water to various municipalities. In the future, actual glacier contraction is expected to influence water availability in the Adige basin.

This study provides an inventory of slope instabilities (500 events in total) that occurred within our study area, without discrimination by size, typology, or epoch. We observed that the majority of such events occurred after the recent deglaciation (post-LIA), suggesting that post-glacial debuttressing and permafrost thaw may predispose to these instabilities. Our database shows how the mountains are rapidly responding to climate change.

The current deglaciation is leading to new risk scenarios affecting mountain infrastructures, such as alpine routes on glaciers. As confirmed by the instability inventory and runout simulations, the alpine tracks crossing the glaciers in our study region cannot be considered outside the potential runout zone of a rockfall and therefore require particular attention and further investigation. The present study provides a comprehensive description of the current situation in the glacial and paraglacial environments, offering crucial information for further risk assessments.

Author contributions
MDB – A, C, D, F, H, I / CC – A, C, E, G, I / MC – A, E, G, I / MP – B, G / DF – A, C, E, G (a) conceptualization; (b) funding acquisition; (c) methodology (including methodological development); (d) investigation (e.g. data collection); (e) resources (provision of data etc.); (f) software (its provision and development); (g) supervision; (h) writing – initial draft; and (i) writing – reviewing and editing.

Funding
This study was supported by the European Union - NextGenerationEU, in the framework of the consortium iNEST - Interconnected Nord-Est Innovation Ecosystem (PNRR, Missione 4 Componente 2, Investimento 1.5 D.D. 1058 23/06/2022, ECS_00000043 – Spoke1, RT1B-03, CUP I43C22000250006). The views and opinions expressed are solely those of the authors and do not necessarily reflect those of the European Union, nor can the European Union be held responsible for them.

Data availability
The outlines produced as part of this research are available upon request.

Declarations

Ethics approval and consent to participate
Not applicable.

Consent for publication
Not applicable.

Competing interests
The authors declare no competing interests.

Received: 1 August 2025 / Accepted: 14 March 2026
Published online: 22 March 2026

References

1. Zemp M, Frey H, Gärtner-Roer I, et al. Historically unprecedented global glacier decline in the early 21st century. J Glaciol. 2015;61:745–62. https://doi.org/10.3189/2015JoG15J017.
2. Hugonnet R, McNabb R, Berthier E, et al. Accelerated global glacier mass loss in the early twenty-first century. Nature. 2021;592:726–31. https://doi.org/10.1038/s41586-021-03436-z.
3. Fischer M, Huss M, Barboux C, Hoelzle M. The New Swiss Glacier Inventory SGI2010: Relevance of Using High-Resolution Source Data in Areas Dominated by Very Small Glaciers. Arct Antarct Alp Res. 2014;46:933–45. https://doi.org/10.1657/1938-4246-46.4.933.
4. Lambrecht A, Kuhn M. Glacier changes in the Austrian Alps during the last three decades, derived from the new Austrian glacier inventory.
5. Knoll C, Kerschner H. A glacier inventory for South Tyrol, Italy, based on airborne laser-scanner data. Ann Glaciol. 2009;50:46–52. https://doi.org/10.3189/172756410790595903.
6. Azzoni RS, D'agata C, Maragno D. (2016) Il Nuovo Catasto dei Ghiacciai Italiani The New Italian Glacier Inventory a cura di / Editors Claudio Smiraglia and Guglielmina Diolaiuti con la collaborazione di / with the scientific and technical support.
7. Paul F, Rastner P, Azzoni RS, et al. Glacier shrinkage in the Alps continues unabated as revealed by a new glacier inventory from Sentinel-2. Earth Syst Sci Data. 2020;12:1805–21. https://doi.org/10.5194/essd-12-1805-2020.
8. Chiarle M, Bondesan A, Carturan L, Scotti R. (2024) Campagna glaciologica annuale dei ghiacciai italiani (2023) Annual glaciological survey of Italian glaciers (2023). Geografia Fisica e Dinamica Quaternaria 47:3–127.
9. Lieb GK. Andreas Kellerer-Pirklbauer (2025) Gletscherbericht_23–24_Bergauf_01–25.
10. Huss M, Bauder A, Linsbauer A. Annual mass balance of Swiss glaciers in 2023/2024.
11. Bondesan A, Francese RG. The climate-driven disaster of the Marmolada Glacier (Italy). Geomorphology. 2023;431:108687. https://doi.org/10.1016/j.geomorph.2023.108687.
12. Wegmann M, Gudmundsson GH, Haeberli W. Permafrost changes in rock walls and the retreat of alpine glaciers: a thermal modelling approach. Permafr Periglac Process. 1998;9:23–33.
13. Paranunzio R, Laio F, Chiarle M, et al. Climate anomalies associated with the occurrence of rockfalls at high-elevation in the Italian Alps. Nat Hazards Earth Syst Sci. 2016;16:2085–106. https://doi.org/10.5194/nhess-16-2085-2016.
14. Ballantyne CK. (2002) Paraglacial geomorphology.
15. Nicholson LI, McCarthy M, Pritchard HD, Willis I. Supraglacial debris thickness variability: impact on ablation and relation to terrain properties. Cryosphere. 2018;12:3719–34. https://doi.org/10.5194/tc-12-3719-2018.

16. Spreafico MC, Sternai P, Agliardi F. Paraglacial rock-slope deformations: sudden or delayed response? Insights from an integrated numerical modelling approach. Landslides. 2021;18:1311–26. https://doi.org/10.1007/s10346-020-01560-x.
17. Noetzli J, Hoelzle M, Haeberli W. (2003) Mountain permafrost and recent Alpine rockfall events: a GIS-based approach to determine critical factors. https://doi.org/10.5167/uzh-33321
18. Krautblatter M, Verleysdonk S, Flores-Orozco A, Kemna A. Temperature-calibrated imaging of seasonal changes in permafrost rock walls by quantitative electrical resistivity tomography (Zugspitze, German/Austrian Alps). J Geophys Res Earth Surf. 2010;115. https://doi.org/10.1029/2008JF001209.
19. Cathala M, Magnin F, Ravanel L, et al. Mapping release and propagation areas of permafrost-related rock slope failures in the French Alps: A new methodological approach at regional scale. Geomorphology. 2024;448:109032. https://doi.org/10.1016/j.geomorph.2023.109032.
20. Haeberli W. Slope stability problems related to glacier shrinkage and permafrost degradation in the Alps. Eclogae Geol Helv. 1997;90:407–14.
21. Cossart E, Braucher R, Fort M, et al. Slope instability in relation to glacial debuttressing in alpine areas (Upper Durance catchment, southeastern France): Evidence from field data and 10Be cosmic ray exposure ages. Geomorphology. 2008;95:3–26. https://doi.org/10.1016/j.geomorph.2006.12.022.
22. Gallach X, Carcaillet J, Ravanel L, et al. Climatic and structural controls on Late-glacial and Holocene rockfall occurrence in high-elevated rock walls of the Mont Blanc massif (Western Alps). Earth Surf Process Landf. 2020;45:3071–91. https://doi.org/10.1002/esp.4952.
23. Kos A, Amann F, Strozzi T, et al. Contemporary glacier retreat triggers a rapid landslide response, Great Aletsch Glacier, Switzerland. Geophys Res Lett. 2016;43. https://doi.org/10.1002/2016GL071708. :12,466 – 12,474.
24. Fischer L, Purves RS, Huggel C et al. (2012) On the influence of topographic, geological and cryospheric factors on rock avalanches and rockfalls in high-mountain areas.
25. Knoflach B, Tussetschläger H, Sailer R, et al. High mountain rockfall dynamics: rockfall activity and runout assessment under the aspect of a changing cryosphere. Geogr Ann Ser A: Phys Geogr. 2021;103:83–102. https://doi.org/10.1080/04353676.2020.1864947.
26. Ritter F, Fiebig M, Muhar A. Impacts of global warming on mountaineering: A classification of phenomena affecting the alpine trail network. Mt Res Dev. 2012;32:4–15. https://doi.org/10.1659/MRD-JOURNAL-D-11-00036.1.
27. Mourey J, Ravanel L, Lambiel C. Climate change related processes affecting mountaineering itineraries, mapping and application to the Valais Alps (Switzerland). Geografiska Annaler. Ser A: Phys Geogr. 2022;104:109–26. https://doi.org/10.1080/04353676.2022.2064651.
28. Volkwein A, Schellenberg K, Labiouse V, et al. Rockfall characterisation and structural protection – a review. Nat Hazards Earth Syst Sci. 2011;11:2617–51. https://doi.org/10.5194/nhess-11-2617-2011.
29. Peruzzetto M, Mangeney A, Grandjean G, et al. Operational estimation of landslide runout: Comparison of empirical and numerical methods. Geosci (Switzerland). 2020;10:1–35. https://doi.org/10.3390/geosciences10110424.
30. Zebisch M, Vaccaro R, Niedrist G, et al. Rapporto sul clima Alto Adige 2018. Bolzano: Eurac Research; 2018.
31. Crespi A, Matiu M, Bertoldi G, et al. A high-resolution gridded dataset of daily temperature and precipitation records (1980–2018) for Trentino-South Tyrol (north-eastern Italian Alps). Earth Syst Sci Data. 2021;13:2801–18. https://doi.org/10.5194/essd-13-2801-2021
32. Stingl Volkmar V and M. Einführung in die Geologie Südtirols: aus Anlass des 32. Internationalen Geologischen Kongresses im Sommer 2004 in Florenz. Bozen: Weise; 2005.
33. Klug L, Froitzheim N. Reuniting the Ötztal Nappe: the tectonic evolution of the Schneeberg Complex. Int J Earth Sci. 2022;111:525–42. https://doi.org/10.1007/s00531-021-02127-4.
34. Barella R, Callegari M, Marin C, et al. Combined Use of Sentinel-1 and Sentinel-2 for Glacier Mapping: An Application Over Central East Alps. IEEE J Sel Top Appl Earth Obs Remote Sens. 2022;15:4824–34. https://doi.org/10.1109/JSTARS.2022.3179050.
35. Galos P, Klug S, Dinale C, R. 20 years of glacier change: the homogenized glacier inventories for south tyrol 1997-2005-2017. Geografia Fisica e Dinamica Quaternaria. 2022;45:171–83. https://doi.org/10.4461/GFDQ.2022.45.6
36. Knoll C, Kerschner H, Heller A, Rastner P. A GIS-based Reconstruction of Little Ice Age Glacier Maximum Extents for South Tyrol, Italy. Trans GIS. 2009;13:449–63. https://doi.org/10.1111/j.1467-9671.2009.01173.x.
37. Shi Y, Liu G, Wang X, et al. Assessing the glacier boundaries in the Qinghai-Tibetan Plateau of China by multi-temporal coherence estimation with Sentinel-1A InSAR. Remote Sens (Basel). 2019;11. https://doi.org/10.3390/rs11040392.
38. Heim A. Der Bergsturz und Menschenleben. Zürich: Fretz und Wasmuth; 1932. p. 218.
39. HSÜ KJ. Catastrophic Debris Streams (Sturzstroms) Generated by Rockfalls. GSA Bull. 1975;86:129–40. https://doi.org/10.1130/0016-7606(1975)86%3C129:CDSSGB%3E2.0.CO;2.
40. Legros F. The mobility of long-runout landslides. Eng Geol. 2002;63:301–31. https://doi.org/10.1016/S0013-7952(01)00090-4.
41. Santi P, Lockyear R, McKenna J, et al. Tools for Predicting Long Runout Landslides. Geosci (Basel). 2025;15. https://doi.org/10.3390/geosciences15020057.
42. Parez S, Aharonov E. Long runout landslides: A solution from granular mechanics. Front Phys. 2015;3. https://doi.org/10.3389/fphy.2015.00080.
43. Corominas J. The angle of reach as a mobility index for small and large landslides. Can Geotech J. 1996;33:260–71. https://doi.org/10.1139/t96-005.
44. Klar A, Aharonov E, Kalderon-Asael B, Katz O. Analytical and observational relations between landslide volume and surface area. J Geophys Res Earth Surf. 2011;116. https://doi.org/10.1029/2009JF001604.
45. Haug ØT, Rosenau M, Rudolf M, et al. Short communication: Runout of rock avalanches limited by basal friction but controlled by fragmentation. Earth Surf Dynam. 2021;9:665–72. https://doi.org/10.5194/esurf-9-665-2021.
46. Wichmann V. The Gravitational Process Path (GPP) model (v1.0) – a GIS-based simulation framework for gravitational processes. Geosci Model Dev. 2017;10:3309–27. https://doi.org/10.5194/gmd-10-3309-2017.
47. Schneider D, Huggel C, Haeberli W, Kaitna R. Unraveling driving factors for large rock–ice avalanche mobility. Earth Surf Process Landf. 2011;36:1948–66. https://doi.org/10.1002/esp.2218.
48. Dijke J, Westen CJ. Rockfall hazard: a geomorphologic application of neighbourhood analysis with ILWIS. ITC J. 1990;1990–1:40–4.

49. Wichmann V, Becht M. In: GeoDynamics, editor. Modeling of geomorphic processes in an alpine catchment. CRC; 2004. pp. 151–67.
50. W NH (1976) Scheidegger AE. 1975. Physical Aspects of Natural Catastrophes. xiii + 289 pp., 53 figs. Elsevier Scientific Publishing Co., Amsterdam, Oxford, New York. Price DFl. 70.00. ISBN 0-444-41216–6. Geol Mag 113:91–91. https://doi.org/10.1017/S0016756800043156
51. Meißl G. Modellierung der Reichweite von Ü FELSSTÜRZEN Fdllbeispiele zur GIS-gestützten Gefahrenbeurteilung dus dem Bayerischen und Tiroler Alpenrdum mit 24 Tabellen und 88 Abbildungen.
52. Fey C, Wichmann V, Zangerl C. Influence of permafrost degradation and glacier retreat on recent high mountain rockfall distribution in the eastern European Alps. Earth Surf Process Landf. 2025;50:e70063. https://doi.org/10.1002/esp.70063.
53. Draebing D, Krautblatter M, Dikau R. Interaction of thermal and mechanical processes in steep permafrost rock walls: A conceptual approach. Geomorphology. 2014;226:226–35. https://doi.org/10.1016/j.geomorph.2014.08.009.
54. Hartmeyer I, Otto J-C. Rockfall, glacier recession, and permafrost degradation: long-term monitoring of climate change impacts at the Open-Air-Lab Kitzsteinhorn, Hohe Tauern. DEUQUA Spec Pub. 2024;5:3–12. https://doi.org/10.5194/deuquasp-5-3-2024.
55. Haeberli W, Paul F, Chiarle M, et al. A surge-type movement at Ghiacciaio del Belvedere and a developing slope instability in the east face of Monte Rosa, Macugnaga, Italian Alps. Nor Geogr Tidsskr. 2002;56. https://doi.org/10.1080/00291950276 0056422.
56. Kääb A, Huggel C, Fischer L, et al. Remote sensing of glacier- and permafrost-related hazards in high mountains: an overview. Nat Hazards Earth Syst Sci. 2005;5:527–54. https://doi.org/10.5194/nhess-5-527-2005.
57. Fischer L, Kääb A, Huggel C, Noetzli J. Geology, glacier retreat and permafrost degradation as controlling factors of slope instabilities in a high-mountain rock wall: the Monte Rosa east face. Nat Hazards Earth Syst Sci. 2006;6:761–72. https://doi.org/10.5194/nhess-6-761-2006.
58. Hartmeyer I, Delleske R, Keuschnig M, et al. Current glacier recession causes significant rockfall increase: The immediate paraglacial response of deglaciating cirque walls. Earth Surf Dyn. 2020;8:729–51. https://doi.org/10.5194/esurf-8-729-2020.
59. Jacquemart M, Weber S, Chiarle M, et al. Detecting the impact of climate change on alpine mass movements in observational records from the European Alps. Earth Sci Rev. 2024;258:104886. https://doi.org/10.1016/j.earscirev.2024.104886.

Websites

60. https://mapview.civis.bz.it/.
61. https://www.geocat.ch/geonetwork/srv/api/records/435522fb-599e-41c0-a7c0-49d922ea6acf.
62. GLIMS: Global Land Ice Measurements from Space.

Publisher's Note